Available online at www.sciencedirect.com
SCIENCE DIRECT®
International Journal of Heat and Mass Transfer 47 (2004) 3769–3782
International Journal of HEAT and MASS TRANSFER
www.elsevier.com/locate/ijhmt

Marangoni convection basic mechanism explanation using the two-point theory (TPT) of mass and heat transfer and the ammonia/water medium

D. Isvoranu [a], M.D. Staicovici [b,*]

[a] Department of Mechanical Engineering, University Politehnica of Bucharest, Splaiul Independentei 113, Bucharest, Romania
[b] SC OVM-ICCPET SA, 236 Vitan Road, 74369 Bucharest, Romania

Received 18 March 2004

Abstract

So far, Marangoni convection is not satisfactorily explained. This work, completing two previous ones, gives the basic mechanism explanation of this effect. Some typical case studies, where Marangoni convection occurs, are regarded through the light of this new theory. The TPT is further used to model a pseudo-Marangoni cell with an ammonia/water absorption process. Special attention has been paid to apply this theory to the cell gas–liquid interface conditions. All modeling results confirm Marangoni convection basic mechanism explanation, which is general. The work emphasizes that TPT is a powerful tool in refined qualitative/quantitative binary two-phase local interaction analysis. Here, it was essential in finding out Marangoni convection true explanation.

1. Introduction

The Marangoni convection stimulation is a practical method used by the thermal absorption technology in the past decades in order that the absorption processes be significantly improved. The literature devoted to this effect is rich, including theoretical and experimental studies on various working fluid-absorbent–surfactant combinations, [1–17]. Besides this, attempts have been made also on explaining its nature. So far, a connection between the absorbent surface tension gradient and induced convection onset and stability is established, but its true mechanism is still not well known.

In a previous paper [18], the basic mechanism of the Marangoni effect is explained, using the two-point theory (TPT) of mass and heat transfer [19] and a new wording of the Laplace equation [20]. Here, further analysis of this topic is done, presenting the recent results of this approach applied to an ammonia/water absorption process in a Marangoni cell.

2. True Marangoni effect mechanism

The common way of inducing Marangoni convection is by obtaining interfacial tension gradients. In mono-component and multi-component media, this is achieved by creating surface temperature gradients (''thermo-capillarity'') and both temperature and working fluid (dissolved surfactant) concentration gradients (''distill-capillarity''), respectively. Several models are proposed to explain distill-capillarity, out of which it can be mentioned that of the surfactant droplet [21], or that of the ''salting (radical)-out'' [22], depending on whether the surfactant exceeds the solubility limit in the absorbent or not. Supposing the surface tension depends on temperature T and working fluid concentration c, $\sigma = \sigma(T, c)$, than, the interfacial tension gradient along a direction x is

* Corresponding author. Tel.: +40-21-211-65-00.
E-mail addresses: dragosis@k.ro (D. Isvoranu), staicovici@dnt.ro (M.D. Staicovici).

0017-9310/$ - see front matter © 2004 Elsevier Ltd. All rights reserved.
doi:10.1016/j.ijheatmasstransfer.2004.04.009

Nomenclature

c	solution mass fraction (dimensionless)
C	absorption heat (J/kg)
d	surfactant droplet half length (m)
c_p	specific heat capacity (J/kg K)
D	mass diffusivity coefficient (m^2/s)
f	figure of merit describing the ipa effect, expressing the magnitude of forces (mass currents) near the ideal point as compared to those far from it
F	force (N)
h	Marangoni cell height (m)
j_r	reduced mass current (dimensionless)
J_v, J_c, J_T	velocity (N/m^2), mass (kg/m^2 s), and heat fluxes (kg K/m^2 s)
l	Marangoni cell half length (m)
$L_{11,r}$	reduced phenomenological length (kg K s/m^2)
L	Marangoni cell characteristic length (m)
Mg	Marangoni number (dimensionless)
$\dot{m}$	gas mass flow rate (kg/s)
p	pressure (N/m^2)
R_1, R_2	surface main curvature radii (m)
t	time (s)
T	temperature (K)
u	liquid velocity along x coordinate (m/s)
v	liquid velocity along y coordinate (m/s)
x, (z)	coordinate along Marangoni cell length (m)
y	coordinate along Marangoni cell high (m)
$(-X_r)$	interaction natural force (J/kg K)

Greek symbols

β	thermal expansion coefficient (1/K)
γ	mass expansion coefficient (dimensionless)
Γ_v, Γ_c, Γ_T	proportionality function in Eq. (14) (N s/m^2, kg/m s and kg/m s, respectively)
Δ	finite difference
λ	thermal conductivity (W/m K)
μ	dynamic viscosity (N s/m^2)
υ	cinematic viscosity (m^2/s)
Π	viscous tensor (N/m^2)
ρ	density (kg/m^3)
σ	surface tension (N/m, J/m^2)
τ	shear stress tensor (N/m^2)
φ_v, φ_c, φ_T	searched functions along direction x: velocity (m/s), mass fraction, (dimensionless) and temperature (K)

Subscripts

P	control volume center
c	critical
e, w, s, n	east, west, south, north
e	interface specific free energy (J/m^2)
f	interface specific force (N/m)
g	gas
i, j, k	variable index
l	liquid
n	current time iteration
r	reduced

$$\frac{\partial\sigma}{\partial x}=\frac{\partial\sigma}{\partial T}\frac{\partial T}{\partial x}+\frac{\partial\sigma}{\partial c}\frac{\partial c}{\partial x} \tag{1}$$

In case of two-component and two-phase interactions, the system is bi-variant and if absorption pressure were established, the equilibrium temperature T and mass fraction c in Eq. (1) depend one of each other. Usually, authors assess distill-capillarity confining to simply evaluate the sign of Eq. (1), only. Additionally, in papers modeling Marangoni convection (e.g. [1,10,17]), surface tension gradient equals the shear stress tensor τ when considering Navier–Stokes equations:

$$\tau_{z_i z_j}=\frac{\partial\sigma}{\partial z_i} \tag{2}$$

where z_i, z_j, $i,j=1,2,3$, are local coordinates for each control volume node at the free surface. As a general remark, the basic factor that brings about the fluid motion in Marangoni convection is not mentioned in any topic published work. For this reason, next we shall give the simple explanation of its true mechanism.

First, in case of a liquid–gas interface, liquid–gas interface pressure difference in a certain point of the fluid free surface, $\Delta p=p_l-p_g$, and surface tension are related by Laplace equation:

$$\Delta p=-\sigma_f\left(\frac{1}{R_1}+\frac{1}{R_2}\right) \tag{3}$$

In Eq. (3), σ_f is the module of the surface tension vector $\vec{\sigma}_f$ considered as a specific force (N/m) acting in the interface tangent plane, and if the interface normal $\vec{n}$ were pointed in order to get out of the liquid, then curvature radii are negative or positive with respect to $\vec{n}$ and from Eq. (3) Δp becomes positive or negative for convex and concave interfaces, respectively, as a classic result.

Now, taking into account the other aspect of the surface tension, which equally might be considered as an interface specific mean free energy (J/m^2), a new wording for the Laplace equation has been found recently [20]

$$\Delta p=\operatorname{div}\vec{\sigma}_e \tag{4}$$

In Eq. (4), Δp has same meaning and values as in Eq. (3) and vector $\vec{\sigma}_e$ (J/m^2), having same module as that of vector $\vec{\sigma}_f$ (N/m) in Eq. (3), $\sigma_e = \sigma_f = \sigma$, is directed towards interface normal (see comment above), or towards the opposite direction, in case of concave or convex surfaces, respectively, and acts in good agreement with the known principle of surface free energy minimization tendency through interface area minimization. Eq. (4) is more general than Eq. (3). In order to proof this statement, it is enough to apply the two equations. to the particular case of an horizontal free surface of a Marangoni cell in a rectangular xy coordinate system, having the normal parallel to the coordinate y, and a non-constant tension gradient with respect to coordinate x, $\frac{\partial\sigma}{\partial x} \neq ct$ in point $(x, 0)$. Results would be different: taking into account that

$$\frac{\partial\sigma_e}{\partial y} = \frac{\partial\sigma_f}{\partial x} \tag{5}$$

Eq. (4) emphasizes the generation of a non-zero fluid pressure gradient with respect to coordinate x, according to ($p_g = ct.$)

$$\frac{\partial p}{\partial x} = \frac{\partial}{\partial x}\left(\frac{\partial\sigma_e}{\partial y}\right) = \frac{\partial}{\partial x}\left(\frac{\partial\sigma_f}{\partial x}\right) = \frac{\partial^2\sigma}{\partial x^2} \neq 0 \tag{6}$$

while Eq. (3) does not, because for R_1 and $R_2 \to \infty$, it results that $\frac{\partial p}{\partial x} = 0$ for any $\vec{\sigma}$ variation [18]. Moreover this result is in good agreement with the "Le Chatelier" principle, the system acting in order to counteract the effect of the $\frac{\partial\sigma}{\partial x} \neq 0$ appearance at interface. Indeed, considering a finite interface control volume as in Fig. 1, Eq. (6) shows that when surface free energy is decreasing in order that $\frac{\partial^2\sigma}{\partial x^2} < 0$, or increasing in order that $\frac{\partial^2\sigma}{\partial x^2} > 0$, then the pressure of the east–west control volume faces with respect to coordinate x will be different, expressed by $\nabla p_B < 0$ or $\nabla p_B > 0$, and a fluid movement will be generated towards positive or negative x coordinate, in order to increase or decrease its free surface, respectively, and preserve its initial specific minimum free energy (see Fig. 3). Further on, taking advantage of Eqs. (4) and (5), fluid motion governed by interfacial tension gradients might be characterized by the following more general property:

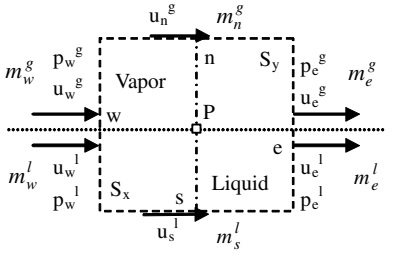

Fig. 1. Interface control volume.

$$\operatorname{grad}(p) = \operatorname{grad}(\operatorname{div}\vec{\sigma}) \tag{7}$$

This mechanism—grad(div$\vec{\sigma}$) → grad(p) → fluid movement—is shown schematically for the salting-out effect [22] and for the Marangoni convection in binary drops in air [12] in Fig. 2a and b, respectively. In case of the ammonia/water system during absorption without additive, Fig. 2a, the crest region of free surface wave becomes ammonia richer, causing surface tension decrease and consequently $p_e - p_w < 0$, so fluid moves downward each crest side. In the wave trough, the reverse happens and fluid moves upward. The two pairs of opposite flows combine in each crest side, resulting in the horizontal opposite flows and the final two counter eddy formation. During the absorption with additives, the radical reverses the effect of ammonia in solution, causing the reverse of fluid movement. Finally, Fig. 2b present the so-called thermo-capillary and distill-capillary effects in mono-component and binary drops in air, condensed on a cool base. The top figures give an incomplete explanation of fluid movement [12]. This work completes it. In case of thermo-capillarity, temperature variation plays the role of ammonia concentration variation, and Fig. 2a without additives applies. In case of distill-capillarity, the lower-temperature evaporating component plays the role of additive, and Fig. 2a with additives applies.

In the following section we shall assess a Marangoni convection from a quantitative point of view, modeling an ammonia/water absorption process in a Marangoni cell. However, prior to do so, first we shall give a simpler mathematical formulation of the induced fluid movement, helpful in our complete understanding of Marangoni convection and further modeling. We consider the cell in Fig. 3 during absorption for an ideal fluid and write equation of Bernoulli in its differential form for the top fluid steady-state moving along the free surface and integrate it between two arbitrary points 1 and x:

$$\int_1^x \mathrm{d}\left(\frac{v^2}{2}\right) = -\int_1^x \frac{\mathrm{d}p}{\rho} \tag{8}$$

For the sake of simplicity, we note that $v(1) \cong 0$ and $\rho \approx ct$. Taking into account Eq. (4) we obtain

$$v(x) = \mp\sqrt{\pm\frac{2}{\rho}\left[\frac{\partial\sigma}{\partial u}(x) - \frac{\partial\sigma}{\partial u}(1)\right]} \tag{9}$$

For a reduced form (index "r"), we put $v_r = v\frac{L}{\upsilon}$ (L—characteristic length, υ—cinematic viscosity) and Eq. (9) becomes

$$v_r(x) = \mp\sqrt{\pm 2[Mg(x) - Mg(1)]} \tag{10}$$

Eq. (10) emphasizes a reduced velocity dependence of a Marangoni number

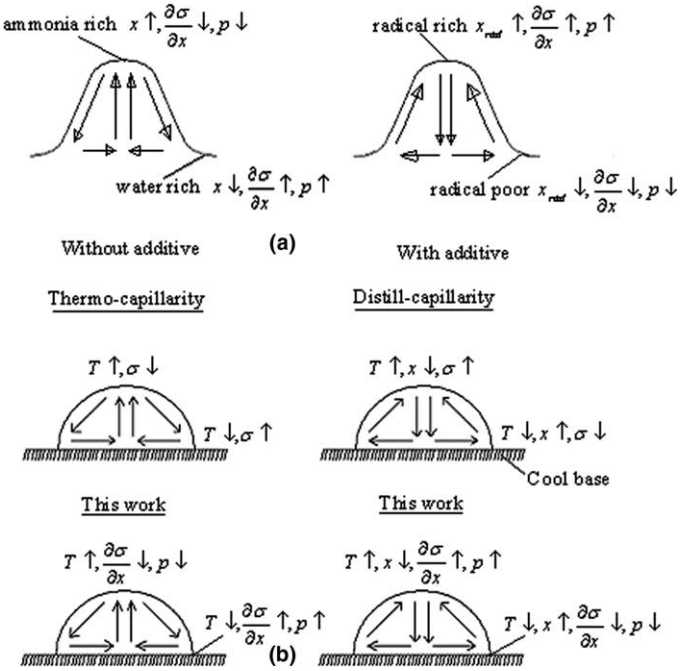

Fig. 2. Surface tension gradient variation → pressure variation → fluid movement mechanism for: (a) salting-out effect [21]; (b) Marangoni convection in binary droplets in air [12].

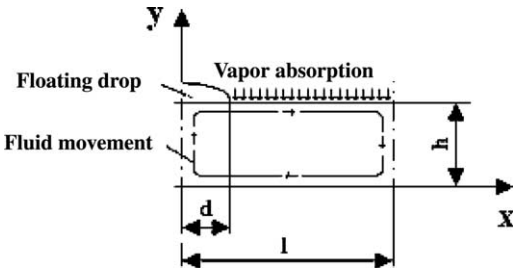

Fig. 3. Schematic of a Marangoni convection cell.

$$Mg = \frac{L^2}{\upsilon^2\rho}\frac{\partial\sigma}{\partial z} \tag{11}$$

Common applications have $|\frac{\partial\sigma}{\partial z}| \approx 10^0 - 10^{-1}$, $L \approx 10^{-2}$, $\upsilon \approx 10^{-6}$, $\rho \approx 10^3$, so that $|Mg| \approx 10^5 - 10^4$. Eq. (9) enables an interfacial tension gradient analysis in order to get a certain induced fluid velocity. To this extent, Eq. (1) was considered for $\sigma = \sigma(c(x))$ only. Analysis of several $\frac{\partial c}{\partial x}$ shapes (linear, polynomial and exponential) revealed that the exponential form got velocities with values met in current applications ($v \approx 10^{-2}$), only. This simple approach suggests an *ipa* behavior [23,24], showing that *ipa* effects accompany Marangoni cells working, and modeling presented in the following section will show this.

Now, taking into account the ideas outlined above, we are able to formulate the Marangoni convection true explanation [18,19]. Indeed, Eqs. (1), (4), (5), (6) and (9) can be considered the key of our problem: *the Marangoni convection is generated by non-constant interfacial tension gradients, which create parallel fluid non-zero pressure gradients, and consequently fluid motion, tending, according to the "Le Chatelier" principle, to counteract in this way the interfacial specific free energy variation. In multicomponent media, this convection is amplified due to the presence of adjacent surface zones with opposite ipa effects, of generation ↔ absorption, which brings about high local non-zero interfacial tension gradients, and further high pressure gradients and fluid motion.* A schematic of the interface Marangoni convection basic mechanism explanation is given in Fig. 4. Here, Fig. 4a and b show the counter and parallel flow formation. They emphasize also the effect of $\frac{\partial\sigma}{\partial x}$ variation, mathematically expressed by

$$\bullet\ \frac{\partial^2\sigma}{\partial x^2} < 0 \ \Rightarrow\ \frac{\partial u}{\partial x} > 0$$

and

$$\bullet\ \frac{\partial^2\sigma}{\partial x^2} > 0 \ \Rightarrow\ \frac{\partial u}{\partial x} < 0. \tag{12}$$

The mechanism of flow deviation is explained next, in Fig. 4c and d. As they indicate, the main flow is deviated by an opposite, secondary flow, towards the bottom of the cell. Obviously, the stronger the secondary flow, the higher the main flow deviation is. Main flow deviation lies at the basis of the eddy formation.

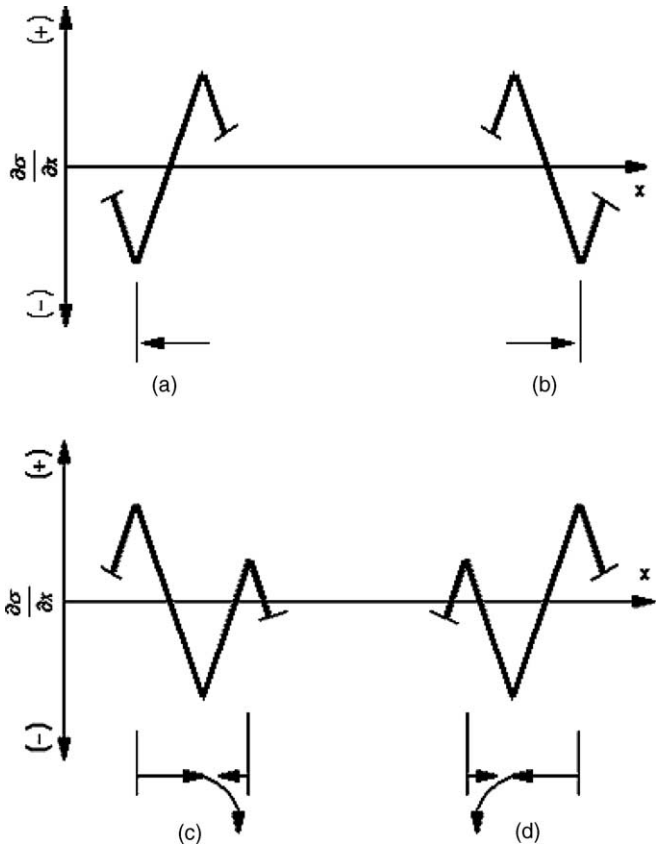

Fig. 4. Schematic of the interface Marangoni convection basic mechanism explanation: (a) counter fluid flow formation $\frac{\partial^2\sigma}{\partial^2 x} > 0 \Rightarrow \nabla_P > 0$; (b) parallel fluid flow formation $\frac{\partial^2\sigma}{\partial^2 x} < 0 \Rightarrow \nabla_P < 0$; (c) parallel fluid flow deviation and clockwise eddy formation; (d) counter fluid flow deviation and counter clockwise eddy formation.

3. Pseudo-Marangoni cell modeling

Induced convection in a pseudo-Marangoni cell, Fig. 3, was modeled with the ammonia/water system. The modeling uses known hydrodynamic, energy and species transport equations for interface and bulk fluid of the cell. Modeling used the TPT for absorption/generation processes at interface [25]. Its first purpose is to analyze with known theoretical tools the Marangoni effect and compare it with the explanation outlined in paper second section. Pseudo-Marangoni cell comes from the fact that no additive effects were accounted for in the convection simulation, meaning that, when absorption starts, the fluid mixture surface located below the "drop" is free of gas absorption, has same surface tension as that of a gas–liquid interface, and absorbing mixture equilibrium is described by its pure ammonia/water equation of state [26].

3.1. Physical model

The governing system of equations comprises Cartesian two-dimensional equation of continuity, Navier–Stokes equations, energy and species transport equations:

$$\begin{aligned}
&\text{Continuity:}\\
&\frac{\partial\rho}{\partial t}+\rho\vec{\nabla}\cdot(\vec{V})=0\\
&\text{Navier–Stokes:}\\
&\rho\frac{\partial\vec{V}}{\partial t}+\rho\vec{V}\cdot\vec{\nabla}(\vec{V})=-\vec{\nabla}p+\vec{\nabla}\cdot\vec{\Pi}+\rho g(\beta\Delta T+\gamma\Delta c)+\vec{F}_g\\
&\text{Energy:}\\
&\rho\frac{\partial T}{\partial t}+\rho\vec{V}\cdot\vec{\nabla}(T)=\frac{1}{c_p}\vec{\nabla}\cdot(\lambda\vec{\nabla}T)\\
&\text{Species:}\\
&\rho\frac{\partial c}{\partial t}+\rho\vec{V}\cdot\vec{\nabla}(c)=\vec{\nabla}\cdot(\rho D\vec{\nabla}c)
\end{aligned}\tag{13}$$

3.2. Numerical model

The system of four partial differential equations was solved numerically, with the help of a CAFFA code

(Computer Aided Fluid Flow Analysis), incorporating the Finite Volume Method. In order to solve the pressure, the SIMPLEX algorithm was used. The simulation domain was discretized by a large enough number of cells in order that the computing accuracy be satifactory. We choosed a rectangular mesh of 96×96 volumes of control. The numerical method is segregated, non-staggered, semi-implicite in space and explicite (Euler) in time, based on a hybride scheme. It applies to the primitive variables velocity, temperature and concentration. Writing the transport equations in the general form

$$\frac{\partial \rho\varphi}{\partial t}+\frac{\partial J_{\varphi,k}}{\partial x_k}=\rho S_\varphi \tag{14}$$

where $J_{\varphi,k}$ is the convective and diffusive flux of the searched function φ along the direction x_k

$$J_{\varphi,k}=\rho u_k\varphi-\Gamma_\varphi\frac{\partial\varphi}{\partial x_k} \tag{15}$$

and integrating over the control volume ΔV, we obtain

$$\begin{aligned}&(\rho_{\mathrm{P}}^{n}\varphi_{\mathrm{P}}^{n}-\rho_{\mathrm{P}}^{n-1}\varphi_{\mathrm{P}}^{n-1})\frac{\Delta V}{\Delta t}+J_{\mathrm{e}}A_{\mathrm{e}}-J_{\mathrm{w}}A_{\mathrm{w}}+J_{\mathrm{n}}A_{\mathrm{n}}-J_{\mathrm{s}}A_{\mathrm{s}}\\&\quad=\overline{\rho S_\varphi}\Delta V\end{aligned} \tag{16}$$

The e, w, n and s indexes hold for the positions of the cell walls, while the uppercase localize the mesh knots. Putting flux $J_{\varphi,k}$ in a discretized form, we obtain a linear algebraic system as

$$a_{\mathrm{P}}\varphi_{\mathrm{P}}=a_{\mathrm{E}}\varphi_{\mathrm{E}}+a_{\mathrm{W}}\varphi_{\mathrm{W}}+a_{\mathrm{N}}\varphi_{\mathrm{N}}+a_{\mathrm{S}}\varphi_{\mathrm{S}}+b_{\mathrm{P}} \tag{17}$$

which was solved by an iterative semi-implicit procedure (SIP).

The boundary and initial conditions, which have made the subject of a through analysis, are given next:

$$\begin{aligned}&1.\ y=h \text{ and } x\in(0,d): u=0, v=0, \frac{\partial T}{\partial y}=0, \frac{\partial c}{\partial y}=0\\&2.\ y=0 \text{ and } x\in(0,l): u=0, v=0, T=293\ \mathrm{K}, \frac{\partial c}{\partial y}=0\\&3.\ x=0 \text{ and } x=l: u=0, \frac{\partial T}{\partial x}=0, \frac{\partial c}{\partial x}=0\end{aligned} \tag{18}$$

The temperature (T), the concentration (c) and the u velocity component can be found at interface, $y=h$ and $x\in(d,l)$, writing the transport equations for the interface control volume (Fig. 1) in the discrete form:

$$\begin{aligned}U_{\mathrm{P}}^{m+1}&=U_{\mathrm{P}}^{m}\left(1-\Delta\dot m\frac{\Delta t}{\rho_{\mathrm{P}}^{m}\Delta V}\right)\\&\quad-\frac{\Delta t}{\rho_{\mathrm{P}}^{m}\Delta V}(\dot m_{\mathrm{e}}^{\mathrm{l}}u_{\mathrm{e}}^{\mathrm{l}}-\dot m_{\mathrm{w}}^{\mathrm{l}}u_{\mathrm{w}}^{\mathrm{l}}+\dot m_{\mathrm{n}}^{\mathrm{g}}u_{\mathrm{n}}^{\mathrm{g}}-\dot m_{\mathrm{s}}^{\mathrm{l}}u_{\mathrm{s}}^{\mathrm{g}})\\&\quad-(p_{\mathrm{e}}^{\mathrm{l}}-p_{\mathrm{w}}^{\mathrm{l}})\frac{S_y}{2}\frac{\Delta t}{\rho_{\mathrm{P}}^{m}\Delta V}\\&\quad+\frac{\Delta t}{\rho_{\mathrm{P}}^{m}\Delta V}\frac{S_y}{2}(\tau_{xx}^{e}-\tau_{xx}^{w})-\frac{\Delta t}{\rho_{\mathrm{P}}^{n}\Delta V}S_x\left(\frac{\mathrm{d}\sigma}{\mathrm{d}x}\right)_{\mathrm{P}}\\T_{\mathrm{P}}^{m+1}&=T_{\mathrm{P}}^{m}-\frac{C}{(c_p)_{\mathrm{P}}^{m}}\dot m_{\mathrm{n}}^{\mathrm{g}}\frac{\Delta t}{\rho_{\mathrm{P}}^{m}\Delta V}\\&\quad+\frac{\Delta t}{\rho_{\mathrm{P}}^{m}\Delta V}\frac{S_y}{2}\left[\left(\frac{\lambda}{c_p}\frac{\partial T}{\partial x}\right)_{\mathrm{e}}-\left(\frac{\lambda}{c_p}\frac{\partial T}{\partial x}\right)_{\mathrm{w}}\right]\\&\quad-\frac{\Delta t}{\rho_{\mathrm{P}}^{m}\Delta V}S_x\left(\frac{\lambda}{c_p}\frac{\partial T}{\partial y}\right)_{\mathrm{s}}\\c_{\mathrm{P}}^{m+1}&=c_{\mathrm{P}}^{m}-(c_{\mathrm{n}}^{\mathrm{g}}-c_{\mathrm{P}}^{m})\dot m_{\mathrm{n}}^{\mathrm{g}}\frac{\Delta t}{\rho_{\mathrm{P}}^{m}\Delta V}\\&\quad+\frac{\Delta t}{\rho_{\mathrm{P}}^{m}\Delta V}\frac{S_y}{2}\left[\left(\rho D\frac{\partial c}{\partial x}\right)_{\mathrm{e}}-\left(\rho D\frac{\partial c}{\partial x}\right)_{\mathrm{w}}\right]\\&\quad-\frac{\Delta t}{\rho_{\mathrm{P}}^{m}\Delta V}S_x\left(\rho D\frac{\partial c}{\partial y}\right)_{\mathrm{s}}\end{aligned} \tag{19}$$

where C is the absorption heat and

$$\begin{aligned}&\Delta\dot m=\dot m_{\mathrm{w}}^{\mathrm{l}}+\dot m_{\mathrm{s}}^{\mathrm{l}}-\dot m_{\mathrm{e}}^{\mathrm{l}}-\dot m_{\mathrm{n}}^{\mathrm{g}}=\frac{\rho_{\mathrm{P}}^{m+1}-\rho_{\mathrm{P}}^{m}}{\Delta t}\Delta V\\&\dot m_{\mathrm{e}}=\dot m_{\mathrm{e}}^{\mathrm{g}}+\dot m_{\mathrm{e}}^{\mathrm{l}};\quad \dot m_{\mathrm{w}}=\dot m_{\mathrm{w}}^{\mathrm{g}}+\dot m_{\mathrm{w}}^{\mathrm{l}}\\&u_{\mathrm{w}}^{\mathrm{g}}=u_{\mathrm{e}}^{\mathrm{g}}=0,\quad \dot m_{\mathrm{w}}^{\mathrm{g}}=\dot m_{\mathrm{e}}^{\mathrm{g}}=0,\quad p_{\mathrm{w}}^{\mathrm{g}}=p_{\mathrm{e}}^{\mathrm{g}},\quad u_{\mathrm{n}}^{\mathrm{g}}=0\\&\dot m_{\mathrm{n}}^{\mathrm{g}}=-j_{\mathrm{r}}[\max(\dot m_{\mathrm{e}}^{\mathrm{l}},0)+\max(\dot m_{\mathrm{w}}^{\mathrm{l}},0)+\max(-\dot m_{\mathrm{s}}^{\mathrm{l}},0)]\\&\left(\frac{\partial T}{\partial y}\right)_{\mathrm{n}}=0;\left(\frac{\partial c}{\partial y}\right)_{\mathrm{n}}=0\\&T_{\mathrm{P}}^{m}\Delta\dot m+\sum_{i=\mathrm{e,w,n,s}}T_i^{m}\dot m_i=\frac{C}{(c_p)_{\mathrm{P}}^{m}}\dot m_{\mathrm{n}}^{\mathrm{g}}\\&c_{\mathrm{P}}^{m}\Delta\dot m+\sum_{i=\mathrm{e,w,n,s}}c_i^{m}\dot m_i=(c_{\mathrm{n}}^{\mathrm{g}}-c_{\mathrm{P}}^{m})\dot m_{\mathrm{n}}^{\mathrm{g}}\end{aligned} \tag{20}$$

The interface gas mass flow rate $\dot m_{\mathrm{n}}^{\mathrm{g}}$ was calculated according to TPT in relation with the reduced absorbed/generated mass flow rate j_{r} (kg gas/kg absorbent mixture) [23,24] and the flow rates traversing faces e, w and s. Also, in equations above we neglected the diffusive terms for the north face in case of T and c, and forces equilibrium at interface results in

$$\tau_{xy}^{\mathrm{s}}=\tau_{xy}^{\mathrm{n}}+\frac{\mathrm{d}\sigma}{\mathrm{d}x} \tag{21}$$

Unlike all previous works (e.g. [1]), considering gas–liquid equilibrium conditions at interface, here for the first time the whole system is supposed to evolve in the cell in a non-equilibrium state, between an initial state, chosen at random (vapor concentration and temperature are $c_{\mathrm{g}}=0.987$ and $T_{\mathrm{g}}=293.15$ K, respectively,

solution initial conditions are $c_l = 0.3$, $T_l = 293.15$ K and the pressure is $p_g = p_l = 1$ bar) and a final one, of an ideal state, given by $p_g = p_l = 1$ bar, $c_g = 0.987$; $c_l = 0.34$, and $T_g = T_l = 293.15$ K. Here, two explanations follow: first, the ideal point is the equilibrium point, thought in a classic meaning, but having different properties with respect to force approaching it (of equilibrium and natural) and second, given that the system is two-component and two-phase, therefore bivariant, and assuming that the two independent variables are absorption pressure and gas mass fraction, kept with constant valued during the whole cell absorption process, $p_g = p_l = 1$ bar = constant, and $c_g = 0.987$ = constant, the ideal point is completely determined. Using the reduced form, according to TPT the mass current absorbed or generated depends on the natural force $(-X_r)$ and phenomenological coefficient $L_{11,r}$ by

$$j_r = L_{11,r}(-X_r)$$

Unlike classic forces, becoming zero in the equilibrium point, the reduced natural force governing the system evolution towards the ideal point, is not, and respects the natural force postulate which emphasizes the ideal point approaching (*ipa*) effect. In our case the *ipa* effect, is plotted in Fig. 5 with respect to solution mass fraction [23]. Mass and heat currents have same *ipa* behavior towards the ideal point.

The thermo-physical and dynamical properties were adjusted every step of time and grid. Next we shall give some information regarding these properties. The surface tension of the ammonia/water mixture was considered linear with respect to the liquid phase mass fraction of pure components [27], according to

$$\sigma_{NH_3/H_2O} = c\sigma_{NH_3} + (1-c)\sigma_{H_2O} \tag{22}$$

where pure component surface tension are functions of temperature, t (K) [28], given by

$$\sigma_{NH_3(H_2O)} = \sigma_{1,NH_3(H_2O)}\left(\frac{t_{c,NH_3(H_2O)} - t}{t_{c,NH_3(H_2O)} - t_1}\right)^{n_{1,NH_3(H_2O)}} \tag{23}$$

In Eq. (23), $\sigma_{1,NH_3(H_2O)}$ is a certain surface tension value, calculated for the temperature $t_{1,NH_3(H_2O)}$ (K), and $t_{c,NH_3(H_2O)}$ (K) and $n_{1,NH_3(H_2O)}$ hold for the critical temperatures and a certain corresponding exponent value of the pure components, respectively. The thermal conductivity of the liquid phase mixture was assessed according to [28]

$$\lambda_{NH_3/H_2O} = c\lambda_{NH_3} + (1-c)\lambda_{H_2O} - 0.72c(1-c) \times (\lambda_{H_2O} - \lambda_{NH_3}) \tag{24}$$

where pure components thermal conductivity is function of liquid temperature, t (°C), given by

$$\lambda_{NH_3(H_2O)} = l_{1,NH_3(H_2O)} + l_{2,NH_3(H_2O)}t + l_{3,NH_3(H_2O)}t^2 \tag{25}$$

and $l_{i,NH_3(H_2O)}$, $i = 1, 2, 3$, are coefficients given in [28]. The dynamic viscosity was assessed in relation with the liquid mass fraction (c) and temperature, t (°C), determining the coefficients $B_{i,j}$, $i = 0, \ldots, 6$, $j = 0, \ldots, 3$, of a double polynomial fit of the known viscosity plot [29]

$$\mu_{NH_3/H_2O} = \sum_{j=0}^{3} t^j \sum_{i=0}^{6} B_{i,j}c^i \tag{26}$$

Additionally, the other thermo-physical and dynamical properties of the ammonia/water mixture (density (ρ), enthalpy, specific heat capacity and expansion coefficients (β, γ)) were calculated from mixture equation of state [26]. The mass diffusivity coefficient (D) was considered function of the liquid mass fraction c, and has been calculated according to the following equation:

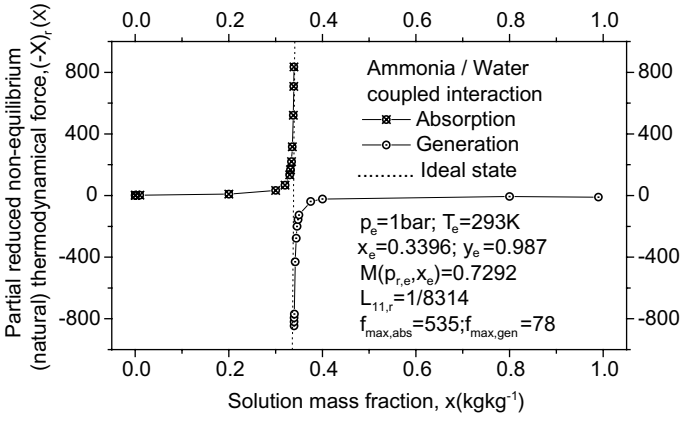

Fig. 5. Natural force behavior around the ideal point of pseudo-Marangoni cell modeling, plotted with respect to absorbent mixture mass fraction.

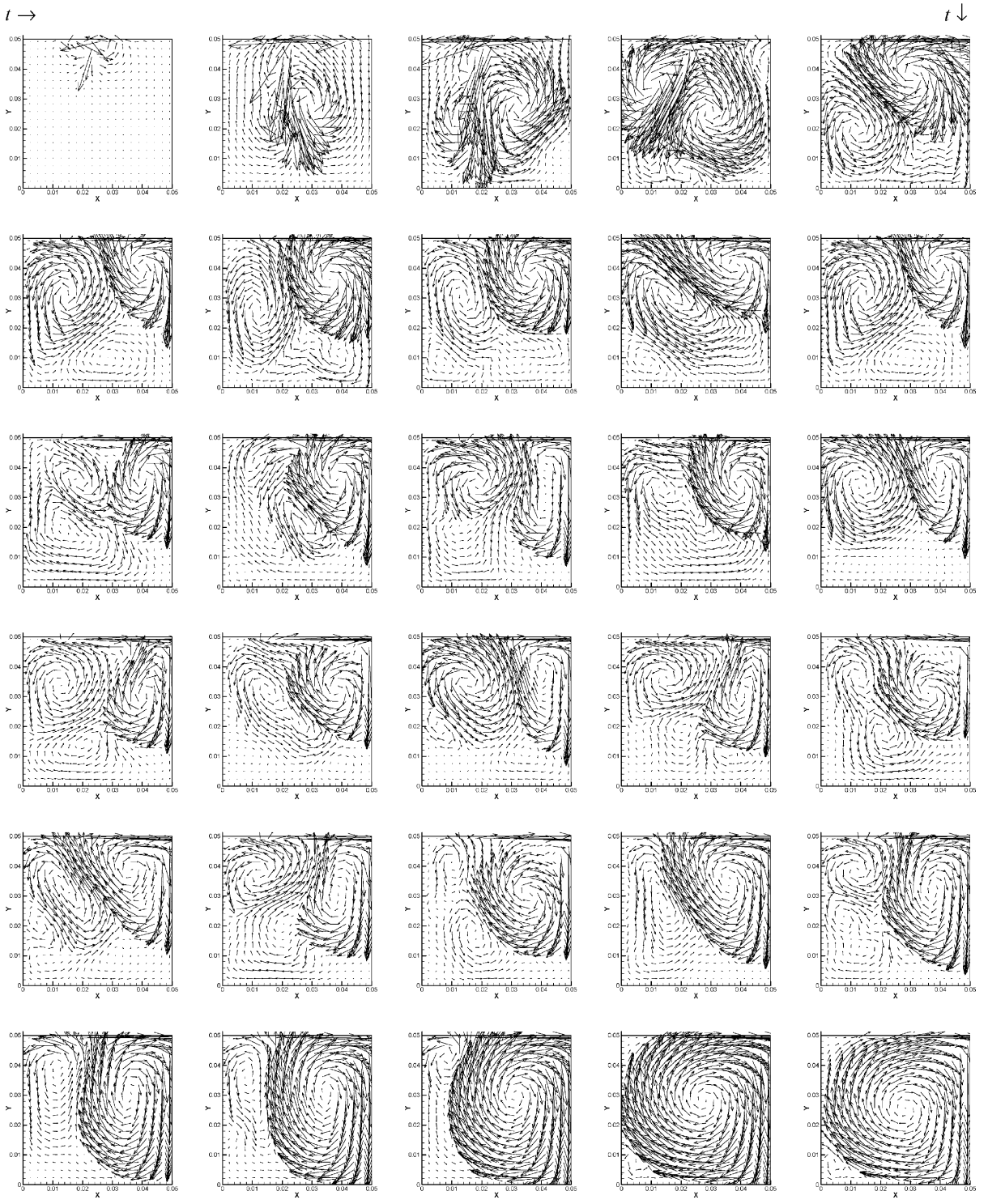

Fig. 6. Marangoni convection film for $(\vec{u}(x,y)+\vec{v}(x,y))$. The top arrows $t\rightarrow$ and $t\downarrow$ indicate time increase in every row and from row to row, respectively. The time can be calculated for each figure in seconds from equations $t_{I\text{–}V}=0.23+(n-1)*0.24$, $n=1,\ldots,25$ and $t_{VI}=6.0+10*0.24*m$, $m=1,\ldots,4$ for the first five rows and for the sixth, respectively. The two last figures characterizes fluid movement for the rest of process, $t\approx 15.6$–240 s and more.

$$D = (3c + 2) \times 10^{-9} \quad (27)$$

Eq. (27) is valid within the range $0.0 \leqslant c \leqslant 0.7$ and has been obtained by linear interpolation of the results of a previous work [30].

4. Modeling results

Results were obtained for cell parameters $l = h = 0.05$ and $d = 0.0125$, Fig. 3. A selection is given in Figs. 6–11. Fig. 6 shows the film of the modeled Marangoni convection for velocity vectors $(\vec{u}(x,y) + \vec{v}(x,y))$, from the first absorption moments, $t \cong 0.23$ s, till the end of the process, $t \geqslant 240$ s. Cell mean ammonia mass fraction evolution is plotted in Fig. 7. In the first minute, the absorption rate is high, and the smaller whirlpools, formed in the beginning, are gradually replaced by a big central one, driving almost all cell fluid. Then, absorption increases little, the ammonia mass fraction asymptotically approaches its ideal point value ($c = 0.34$), and the big central whirlpool dominates the whole fluid movement. When absorption starts, an ammonia mass fraction and temperature difference appears between

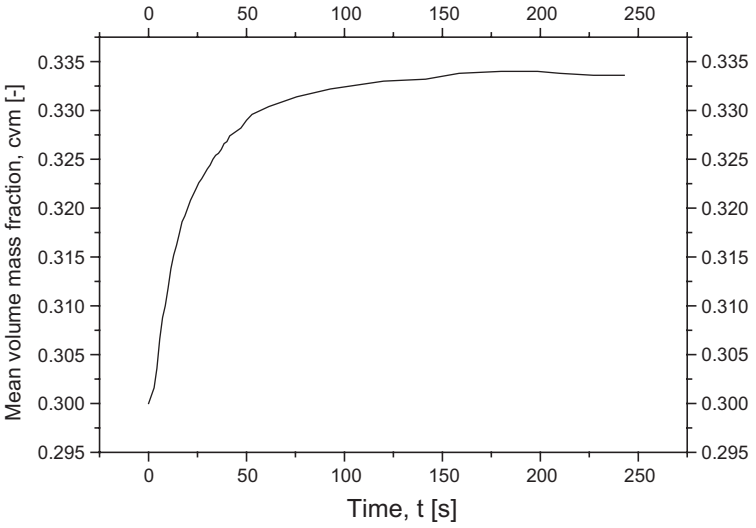

Fig. 7. Ammonia mass fraction evolution during absorption in the modeled ammonia/water pseudo-Marangoni cell convection.

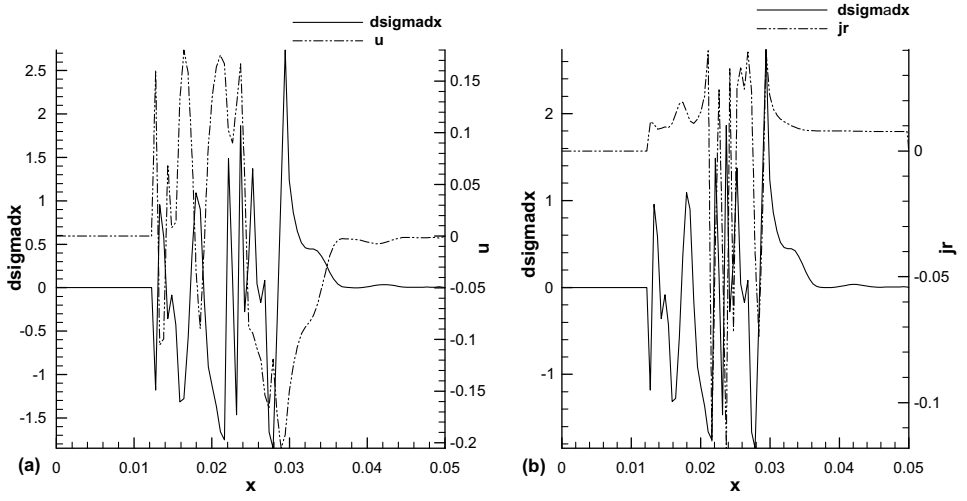

Fig. 8. First moments of absorption modeling ($t = 0.23$ s): (a) $\frac{\partial\sigma(x)}{\partial x}$ and $u(x,h)$; (b) $\frac{\partial\sigma(x)}{\partial x}$ and $j_r(x)$.

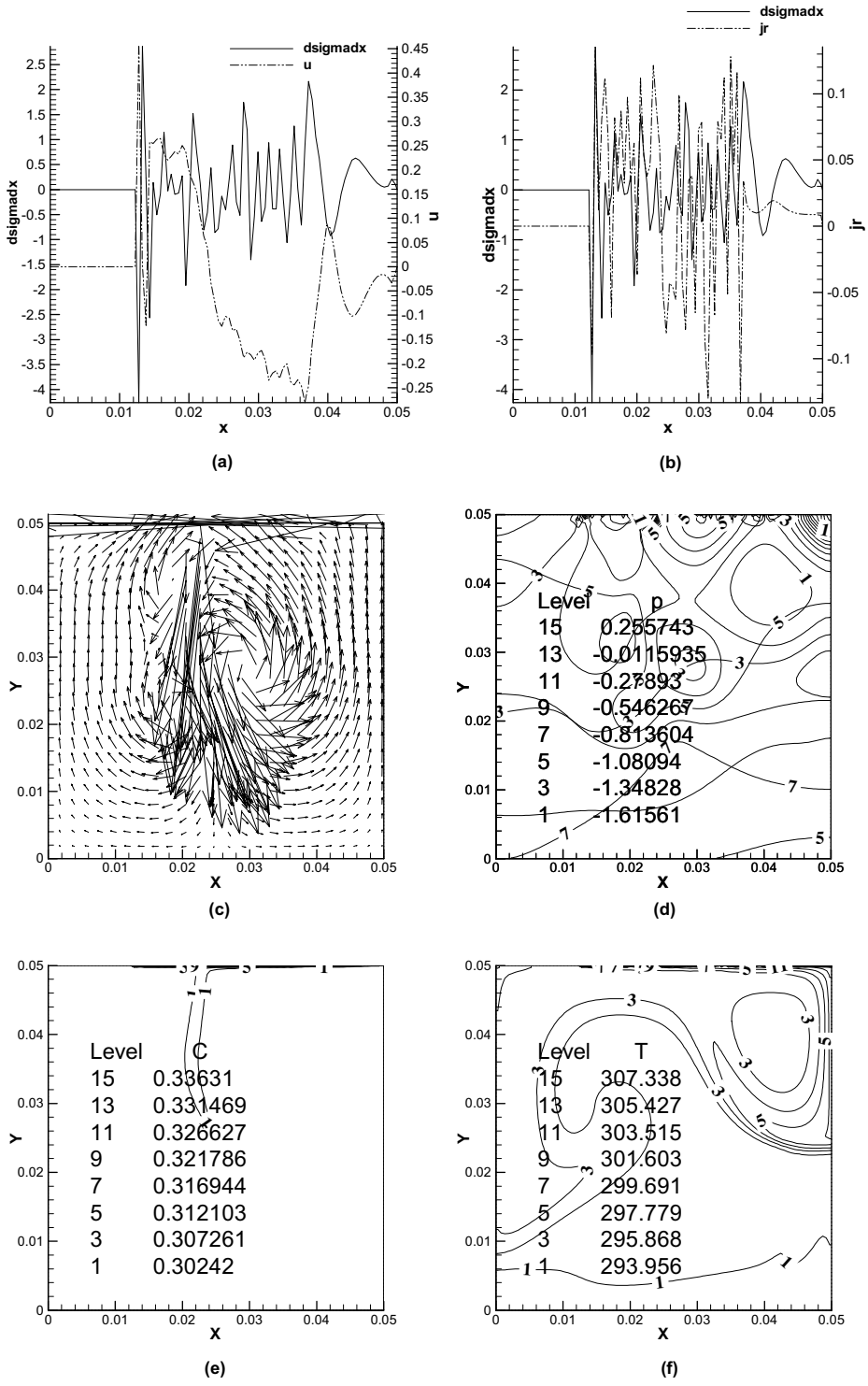

Fig. 9. Modeling results of the absorption ammonia/water pseudo-Marangoni cell (time 0.47 s): (a) $\frac{\partial\sigma(x)}{\partial x}$ and $u(x,h)$; (b) $\frac{\partial\sigma(x)}{\partial x}$ and $j_r(x)$; (c) $(\vec{u}(x,y)+\vec{v}(x,y))$; (d) $p(x,y)$; (e) $c(x,y)$; (f) $T(x,y)$.

fluid surfaces located under "drop" and the adjacent absorbing free surface (see pseudo-Marangoni cell explanation, given in Section 3), causing unbalanced surface tension gradients and top fluid movement re-

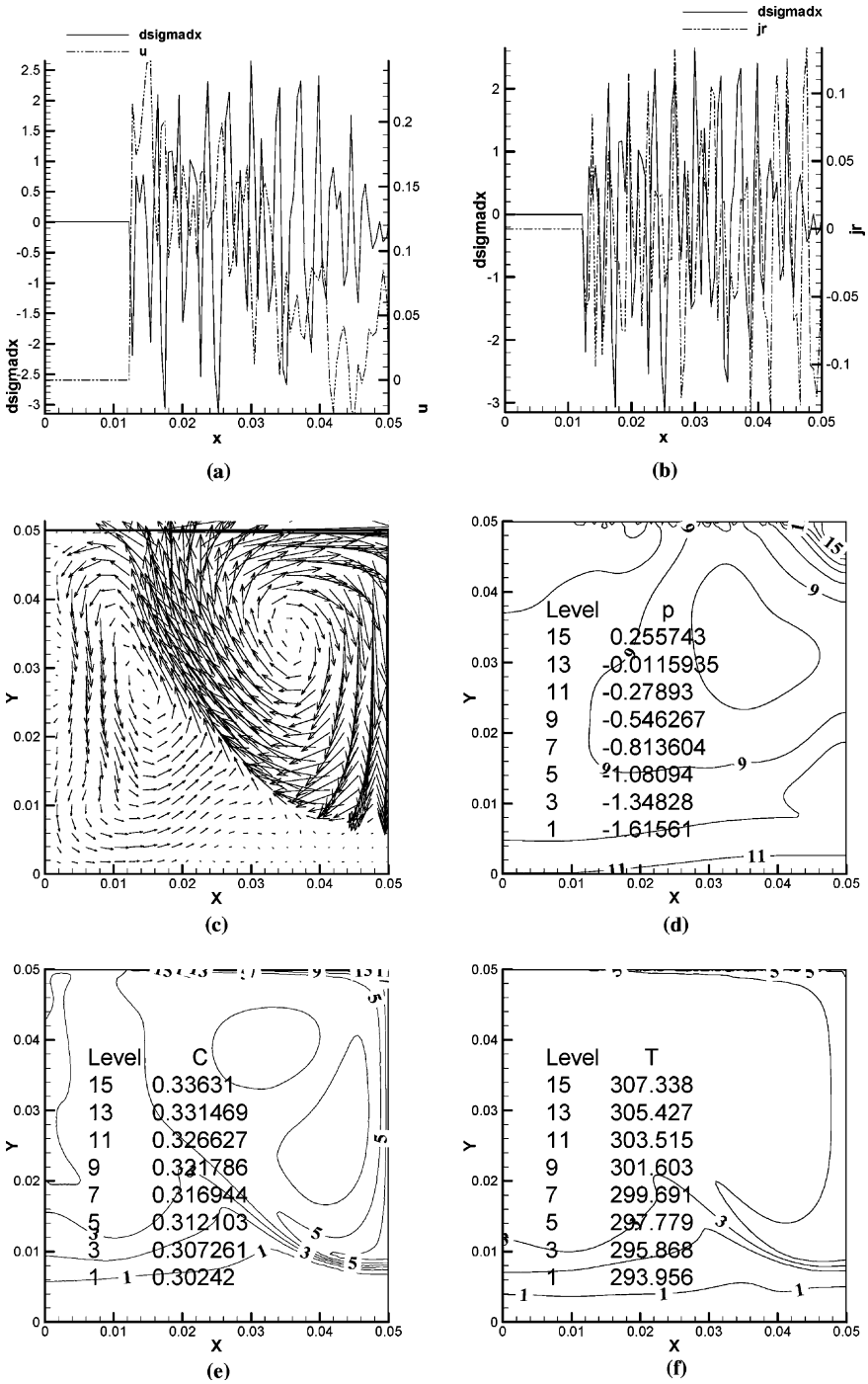

Fig. 10. Modeling results of the absorption ammonia/water pseudo-Marangoni cell (time 5.75 s): (a) $\frac{\partial\sigma(x)}{\partial x}$ and $u(x,h)$; (b) $\frac{\partial\sigma(x)}{\partial x}$ and $j_r(x)$; (c) $(\vec{u}(x,y)+\vec{v}(x,y))$; (d) $p(x,y)$; (e) $c(x,y)$; (f) $T(x,y)$.

lease. First moments of absorption and fluid movement are described by Figs. 6 and 8. Velocity u rigorously obeys inequalities (12) with respect to $\frac{\partial\sigma(x)}{\partial x}$ variation, Fig. 8a, strictly determined by the $j_r(x)$ variation, Fig. 8b. Figs. 9–11, obtained for three different absorption times (corresponding to absorption beginning, middle

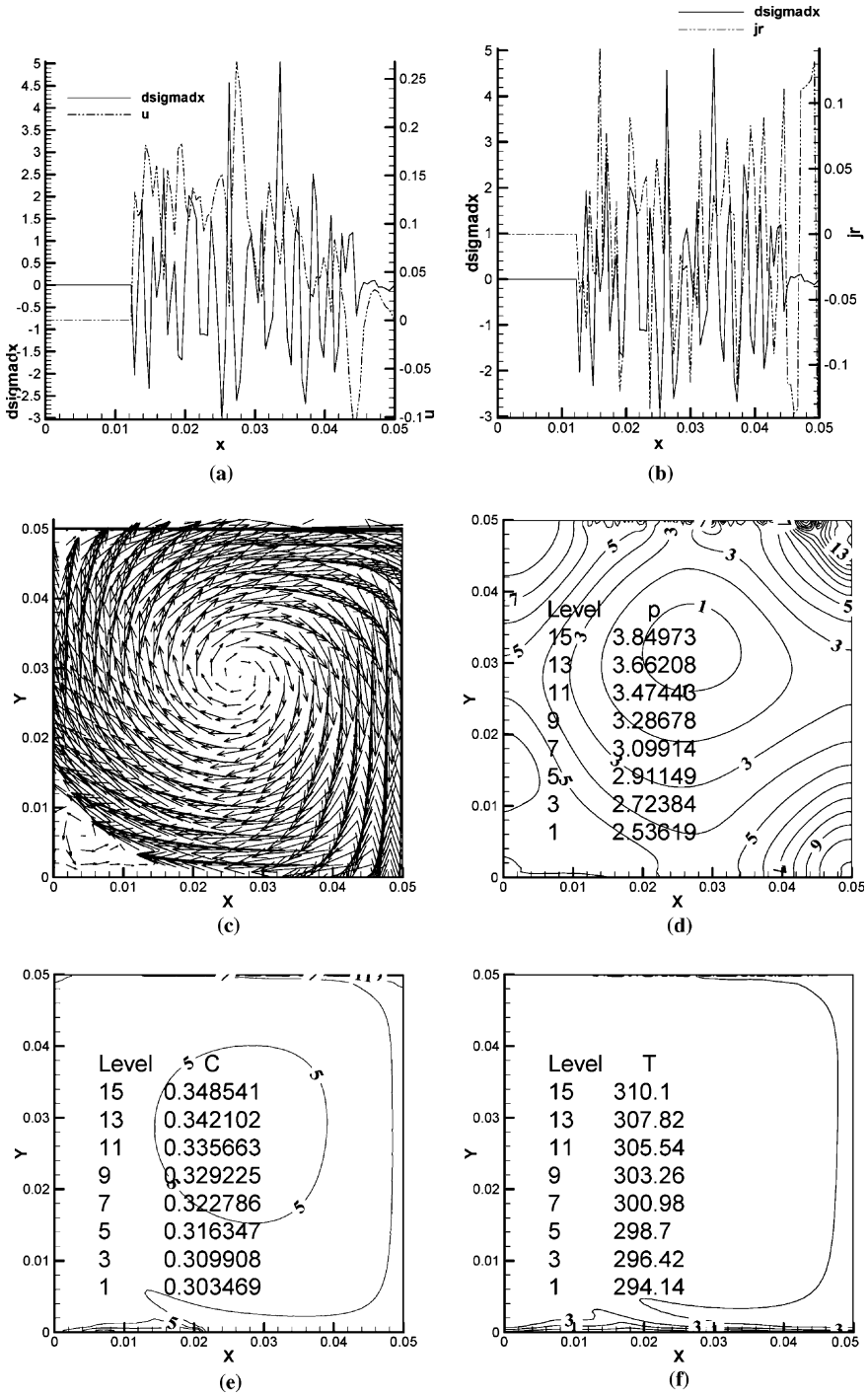

Fig. 11. Modeling results of the absorption ammonia/water pseudo-Marangoni cell (time 15.6 s): (a) $\frac{\partial\sigma(x)}{\partial x}$ and $u(x,h)$; (b) $\frac{\partial\sigma(x)}{\partial x}$ and $j_r(x)$; (c) $(\vec{u}(x,y)+\vec{v}(x,y))$; (d) $p(x,y)$; (e) $c(x,y)$; (f) $T(x,y)$.

and end of process) and noted each with (a)–(f), represent functions $\frac{\partial\sigma(x)}{\partial x}$ and $u(x,h)$, $\frac{\partial\sigma(x)}{\partial x}$ and $j_r(x)$ $(\vec{u}(x,y)+\vec{v}(x,y))$, $p(x,y)$, $c(x,y)$ and $T(x,y)$, respectively. An interpretation of the plotted results follows, with emphasis of Marangoni convection explanation, given in Section 2:

(1) $j_r(x)$ plots reveal the occurrence of *ipa* effects, characterized by figures of merit having magnitude order of $f_{abs,gen} \approx 10^1$–10^2.
(2) Surprisingly for an absorption cell, its free surface suffers not only absorption processes, $j_r > 0$, but generation ones also, $j_r < 0$; both processes occur either simultaneously in adjacent places, or in same place but different times; the generation process diminishes absorption efficiency, but this is the prize paid by the Marangoni cell for producing fluid mechanical work (convection); from this point of view, bubble flow based absorbers stimulate more absorption *ipa* effect appearance, receive mechanical work and for this reason they might be more efficient.
(3) Generally, $\frac{\partial\sigma(x)}{\partial x} > 0$ for $j_r \geqslant 0$ and $\frac{\partial\sigma(x)}{\partial x} < 0$ for $j_r < 0$; although this is not rigorously verified, the reduced mass current j_r fundamentally influences $\frac{\partial\sigma(x)}{\partial x}$ variation and consequently fluid movement.
(4) High surface tension gradients play the most important role in Marangoni convection.
(5) The Marangoni basic mechanism, outlined in Fig. 4a–d and by inequalities (12), is rigorously verified for all results. This can be checked in Figs. 8a–11a, and Figs. 9c–11c, including here the eddy formation process.

From the above it results that TPT is a powerful, essential tool in refined qualitative/quantitative binary two-phase local interaction analysis. Also, the results suggest that Marangoni convection could be obtained without surfactant use, not only in absorption processes, as we already showed through the present modeling, but also in generation of binary processes, if adequate cells were constructed, which stimulate by their geometry an initial surface tension gradient appearance, because, once started, the Marangoni convection is capable to evolve by itself (to be self maintained). Being independent of the refrigerant/absorbent working combination, of whether a surfactant is dissolved or not in an absorbent, of whether the processes are of thermo-capillarity or of distill-capillarity, the Marangoni convection basic mechanism explanation, outlined in the previous papers [18,25] and in this one, is general.

5. Conclusions

So far, Marangoni convection is not satisfactorily explained. This work, completing two previous works, gives the basic mechanism explanation of this effect. Some typical case studies, where Marangoni convection occurs, are regarded through the light of this new theory. The TPT is used further to model a pseudo-Marangoni cell with an ammonia/water absorption process. Modeling results specific conclusions follow:

- $j_r(x)$ plots reveal the occurrence of *ipa* effects, characterized by figures of merit having magnitude order of $f_{abs,gen} \approx 10^1$–10^2.
- Surprisingly for an absorption cell, its free surface suffers not only absorption processes, $j_r > 0$, but generation ones also, $j_r < 0$; both processes occur either simultaneously in adjacent places, or in same place but different times.
- The generation process diminishes absorption efficiency, but this is the prize paid by the Marangoni cell for producing fluid mechanical work (convection); from this point of view, bubble flow based absorbers stimulate more absorption *ipa* effect appearance, receive mechanical work and for this reason they might be more efficient.
- High surface tension gradients play the most important role in Marangoni convection.
- All modeling results confirm Marangoni convection basic mechanism explanation, which is general.
- The work emphasizes that TPT is a powerful tool in the refined qualitative/quantitative binary two-phase local interaction analysis. Here, it was essential in finding out Marangoni convection true explanation.

References

[1] D.-H. Rie, T. Kashiwagi, Computer simulation of vapor absorption enhancement into H_2O/LiBr absorbent by Marangoni convection, JSME-Int. J. III 34 (3) (1991) 355–361.
[2] E. Hihara, T. Saito, Effect of surfactant on falling film absorption, Rev. Int. Froid 16 (5) (1994) 339–346.
[3] M. Nordgren, F. Setterwall, An experimental study of the effects of surfactant on a falling liquid film, Int. J. Refr. 19 (5) (1996) 310–316.
[4] R. Möller, K.F. Knoche, Surfactants with NH_3–H_2O, Int. J. Refr. 19 (5) (1996) 317–321.
[5] K.J. Kim, N.S. Berman, B.D. Word, The interfacial turbulence in falling film absorption: effects of additives, Int. J. Refr. 19 (5) (1996) 322–330.
[6] L. Hoffmann et al., Experimental investigation of heat transfer in a horizontal tube falling film absorber with aqueous solutions of LiBr with and without surfactants, Int. J. Refr. 19 (5) (1996) 331–341.
[7] A. Beutler et al., Surfactants and fluid properties, Int. J. Refr. 19 (5) (1996) 342–346.
[8] Y.T. Kand, A. Akisawa, T. Kashiwagi, Visualization and model development of Marangoni convection in NH_3–H_2O system, Int. J. Refr. 22 (1999) 640–649.
[9] V.-M. Ha, Onset of Marangoni instability of a two-component evaporating droplet, Int. J. Heat Mass Transfer 45 (26) (2002) 5143–5158.
[10] Ch. Boyadjiev, I. Halatchev, Nonlinear mass transfer and Marangoni effect in gas–liquid systems, Int. J. Heat Mass Transfer 41 (1) (1998) 197–202.
[11] O. Velde et al., Numerical investigation of the Lorentz force influenced Marangoni convection relevant to

aluminium surface alloying, Int. J. Heat Mass Transfer 44 (14) (2001) 2751–2762.
[12] F.L.A. Ganzevles, C.W.M. Van der Geld, Marangoni convection in binary drops in air cooled from below, Int. J. Heat Mass Transfer 41 (10) (1998) 1293–1312.
[13] Y.L. Yao, F. Liu, W.R. Hu, How to determine critical Marangoni number in half floating zone convection, Int. J. Heat Mass Transfer 39 (12) (1996) 2539–2544.
[14] M. Li, D. Zang, T. Zhu, Instability of the Marangoni convection in a liquid bridge with liquid encapsulation under microgravity conditions, Int. J. Heat Mass Transfer 45 (1) (2002) 157–164.
[15] H. Daiguji, E. Hihara, T. Saito, Mechanism of absorption enhancement by surfactant, Int. J. Heat Mass Transfer 40 (8) (1997) 1743–1752.
[16] V. Kumar et al., Effect of thermo-capillary convection in an industrial Czochralsky crucible: numerical simulation, Int. J. Heat Mass Transfer 46 (9) (2003) 1641–1652.
[17] A. Bahloul et al., Effect on surface tension on convection in a binary fluid layer under a zero gravity environment, Int. J. Heat Mass Transfer 46 (10) (2003) 1759–1771.
[18] M.D. Staicovici, D. Isvoranu, The Marangoni convection: a two-point theory of mass and heat transfer and Laplace equation new wording approach, in: Proc. 21th Int. Congr. of Refrigeration, Washington, 17–22 August 2003.
[19] M.D. Staicovici, A non-equilibrium phenomenological (two-point) theory of mass and heat transfer. Forces, system-source interactions and thermodynamic cycle application, Int. J. Therm. Sci. 41 (2002) 737–752.
[20] M.D. Staicovici, A variational numerical and analytical approach of the capillary rise effect, Rev. Roum. Sci. Techn.-Méc. 43 (1) (1998) 85–99.
[21] T. Kashiwagi, Basic mechanism of absorption heat and mass transfer enhancement by the Marangoni effect, Newsletter, IEA Heat Pump Center 6 (4) (1988) 2–6.
[22] M. Hozawa et al., Marangoni convection during steam absorption into aqueous LiBr solution with surfactant, J. Chem. Eng. Jpn. 24 (2) (1991) 209–214.
[23] M.D. Staicovici, A non-equilibrium phenomenological theory of the mass and heat transfer in physical and chemical interactions. Part I—Theory and its application to NH_3/H_2O and other working systems, Int. J. Heat Mass Transfer 43 (22) (2000) 4153–4173.
[24] M.D. Staicovici, A non-equilibrium phenomenological theory of the mass and heat transfer in physical and chemical interactions. Part II—Modelling of the NH_3/H_2O bubble absorption, analytical study of absorption and experiments, Int. J. Heat Mass Transfer 43 (22) (2000) 4175–4188.
[25] M.D. Staicovici, D. Isvoranu, The Marangoni convection explanation: a two-point theory (TPT) of mass and heat transfer and new Laplace equation approach. Accepted for ICHMT (Int. Symposium on Advances in computational Heat Transfer), CHT-04, Norway, April 2004.
[26] B. Ziegler, C. Trepp, Equation of state for ammonia/water mixtures, Int. J. Refrig. 7 (1984) 101–106.
[27] Tables and diagrams for the refrigeration industry. Thermodynamic and physical properties, ammonia/water. IIR, 1994.
[28] M. Geana, P. Ionescu, A. Vais, G. Ivanus, Fluid Physical Properties (in Romanian), Technical Publishing House, Bucharest, 1993.
[29] F. Chiriac, V. Cartas, Cooling Plants, Project Design Guide, Annex for Cooling Agents and Thermodynamic and Physical Properties (in Romanian), Civil Engineering Institute, Bucharest, 1972.
[30] M. Kojima, T. Kashiwagi, Mass diffusivity measurements for ammonia vapor absorption processes, in: Proc. of the 19th Int. Congr. of Refrigeration, Hague, IV (a), 1995, pp. 353–360.